Effects of a far-infrared photon cavity field on the magnetization of a square quantum dot array

Vidar Gudmundsson [1,*] Vram Mughnetsyan [2,†] Nzar Rauf Abdullah [3,4] Chi-Shung Tang [5,‡]
Valeriu Moldoveanu [6,§] and Andrei Manolescu [7,‖]

[1]*Science Institute, University of Iceland, Dunhaga 3, IS-107 Reykjavik, Iceland*
[2]*Department of Solid State Physics, Yerevan State University, Alex Manoogian 1, 0025 Yerevan, Armenia*
[3]*Physics Department, College of Science, University of Sulaimani, 501 Sulaimani, Kurdistan Region, Iraq*
[4]*Computer Engineering Department, College of Engineering,*
Komar University of Science and Technology, Sulaimani 46001, Kurdistan Region, Iraq
[5]*Department of Mechanical Engineering, National United University, Miaoli 36003, Taiwan*
[6]*National Institute of Materials Physics, PO Box MG-7, Bucharest-Magurele, Romania*
[7]*Department of Engineering, Reykjavik University, Menntavegur 1, IS-102 Reykjavik, Iceland*

The orbital and spin magnetization of a cavity-embedded quantum dot array defined in a GaAs heterostructure are calculated within quantum-electrodynamical density-functional theory. To this end, a gradient-based exchange-correlation functional recently employed for atomic systems is adapted to the hosting two-dimensional electron gas submitted to an external perpendicular homogeneous magnetic field. Numerical results reveal the polarizing effects of the cavity photon field on the electron charge distribution and nontrivial changes of the orbital magnetization. We discuss its intertwined dependence on the electron number in each dot, and on the electron-photon coupling strength. In particular, the calculated dispersion of the photon-dressed electron states around the Fermi energy as a function of the electron-photon coupling strength indicates the formation of magnetoplasmon-polaritons in the dots.

I. INTRODUCTION

Research into the influence of cavity photon modes on electron transport through nanoscale systems [1], optical properties of two-dimensional (2D) electron systems [2–4], quasiparticle excitation in light-matter systems [5–8], or processes in chemistry [9–12], has been gaining attention in the last three decades, just to cite the work of few groups involved. The diverse systems and their phenomena have been theoretically described by a multitude of methods ranging from simple toy models [13,14], nonequilibrium Green's functions [15], and master equations of various types. In the more complex models with few to many charged entities, traditional approaches to many-body theory, or configuration interactions (exact diagonalization in many-body Fock space), have been used [16], but relatively recently, density functional theory approaches have been appearing [17–20].

The foundation of the approach lies in combining the polarization of a Dirac or a Schrödinger field and the vector potential for a photon field by solving two coupled nonlinear differential equations for the evolution without explicitly referring to many-body wave functions of the coupled system [17]. The procedure has been illustrated excellently by Flick *et al.* in a more recent publication [19].

Only very recently, an explicit analytical gradient-based functional exchange-correlation energy functional derived from the adiabatic-connection fluctuation-dissipation theorem [21] has been published [22]. Interestingly, the development of this functional is closely related to earlier work on the van der Waals and Casimir interactions in complex molecular systems and macroscopic bodies [23,24].

Experiments have shown that a two-dimensional electron gas (2DEG) in a GaAs heterostructure is an ideal experimental system to achieve strong electron-photon coupling in a far-infrared (FIR) cavity [3]. Motivated by this fact, we suitably modify the exchange and correlation energy functional and extend it to a square periodic lattice of quantum dots formed in a 2DEG and subjected to perpendicular homogeneous magnetic field. We apply it to investigate the influences of the coupling to a cavity photon mode on the orbital magnetization of the system. This choice of applications has two intertwined reasons: First, the orbital and spin components of the magnetization are equilibrium quantities that do not invoke any need of calculations of the dynamical properties of the system [25,26]. Second, the magnetization is thus an appropriate experimental equilibrium quantity that could be used to control and assist in the development of quantum-electrodynamical density functional theory (QEDFT) approaches, that are needed for wide areas of applications in physics and chemistry.

*vidar@hi.is
†vram@ysu.am
‡cstang@nuu.edu.tw
§valim@infim.ro
‖manoles@ru.is

In addition, it is clear that the polarization of the electron density by the cavity-photon field must change the orbital magnetization of the electron system, and as GaAs systems are ideal to enable tuning of the electron-photon coupling strength, we do the calculations for GaAs parameters [3].

In the Sec. II, we introduce the computational model for the 2DEG, collecting all technical, but important, details on the local spin density field theoretical (LSDA) approach for the electron-electron Coulomb interaction in Appendix A. Also, details about the construction of the gradient-based nonlocal exchange and correlation functional for the electron-photon interaction are given in Appendix B. The results are presented in Sec. III, and conclusions are summarized in Sec. IV.

II. MODEL

We model electrons in a 2D square periodic lattice of quantum dots defined by the potential

$$V_{\text{per}}(\boldsymbol{r}) = -V_0 \left[\sin\left(\frac{g_1 x}{2}\right) \sin\left(\frac{g_2 y}{2}\right) \right]^2, \quad (1)$$

with $V_0 = 16.0$ meV. The dot square array is defined by the lattice vectors $\boldsymbol{R} = n\boldsymbol{l}_1 + m\boldsymbol{l}_2$, where $n, m \in \boldsymbol{Z}$. Its unit vectors are $\boldsymbol{l}_1 = L\boldsymbol{e}_x$ and $\boldsymbol{l}_2 = L\boldsymbol{e}_y$. The reciprocal lattice is spanned by $\boldsymbol{G} = G_1\boldsymbol{g}_1 + G_2\boldsymbol{g}_2$ with $G_1, G_2 \in \boldsymbol{Z}$ with the unit vectors

$$\boldsymbol{g}_1 = \frac{2\pi \boldsymbol{e}_x}{L} \quad \text{and} \quad \boldsymbol{g}_2 = \frac{2\pi \boldsymbol{e}_y}{L}, \quad (2)$$

where $L = 100$ nm. A local spin-density functional theory (LSDFT) approach is used to describe the mutual Coulomb interactions of the electrons in the presence of a homogeneous external magnetic field $\boldsymbol{B} = B\hat{\boldsymbol{e}}_z$ perpendicular to the plane of the 2DEG. To fulfill the commensurability conditions of the lattice length of the dot lattice and the characteristic length scale associated with the magnetic field $l = (\hbar c/(eB))^{1/2}$ [27–29], we use a state basis constructed by Ferrari [30] in the symmetric gauge, and used previously by Silberbauer [31] and Gudmundsson and Gerhardts [32]. The QEDFT Hamiltonian of the Coulomb interacting electrons in a photon cavity is

$$H = H_0 + H_{\text{Zee}} + V_{\text{H}} + V_{\text{per}} + V_{\text{xc}} + V_{\text{xc}}^{\text{EM}}, \quad (3)$$

where the last term describing the coupling of the electrons to the cavity photon field will be described in detail later. H_0 is the Hamiltonian of free 2D electrons in the external magnetic field:

$$H_0 = \frac{1}{2m^*}\boldsymbol{\pi}^2, \quad \text{with} \quad \boldsymbol{\pi} = \left(\boldsymbol{p} + \frac{e}{c}\boldsymbol{A}\right). \quad (4)$$

In the symmetric gauge, the vector potential is $\boldsymbol{A} = (B/2)(-y, x)$. The wave functions of the Ferrari basis [30] are the Kohn-Sham eigenfunctions of H_0 denoted by $\phi_{n_l}^{\mu\nu}(\boldsymbol{r})$ with $n_l = 0, 1, 2, \cdots$ a Landau band index and $\mu = (\theta_1 + 2\pi n_1)/p$, $\nu = (\theta_2 + 2\pi n_2)/q$, with $n_1 \in I_1 = \{0, \ldots, p-1\}$, $n_2 \in I_2 = \{0, \ldots, q-1\}$, and $\theta_i \in [-\pi, \pi]$. pq is the number of magnetic flux quanta $\Phi_0 = hc/e$ flowing through a unit cell of the lattice. We denote the eigenfunctions of the total Hamiltonian with $\psi_{\beta\boldsymbol{\theta}\sigma}(\boldsymbol{r})$, where $\sigma = \{\uparrow\downarrow\}$ indicates the z component of the spin, $\boldsymbol{\theta} = (\theta_1, \theta_2)$ is the location in the unit cell of the reciprocal lattice, and β stands for all remaining quantum numbers. In each point of the reciprocal lattice, $\boldsymbol{\theta}$,

the eigenfunctions $\phi_{n_l}^{\mu\nu}$ and $\psi_{\beta\boldsymbol{\theta}\sigma}$ form complete orthonormal bases if $(\mu, \nu) \neq (\pi, \pi)$ for all $(n_1, n_2) \in I_1 \times I_2$.

The Hartree part of the Coulomb interaction is

$$V_{\text{H}}(\boldsymbol{r}) = \frac{e^2}{\kappa} \int_{\boldsymbol{R}^2} d\boldsymbol{r}' \frac{\Delta n(\boldsymbol{r}')}{|\boldsymbol{r} - \boldsymbol{r}'|}, \quad (5)$$

with $\Delta n(\boldsymbol{r}) = n(\boldsymbol{r}) - n_{\text{b}}$, where $+en_{\text{b}}$ is the homogeneous positive background charge density needed to maintain the total system charge neutral. We consider the positive background charge to be located in the plane of the 2DEG. The electron density is

$$n_e(\boldsymbol{r}) = n_\uparrow(\boldsymbol{r}) + n_\downarrow(\boldsymbol{r})$$

$$= \frac{1}{(2\pi)^2} \sum_{\beta\sigma} \int_{-\pi}^{\pi} d\boldsymbol{\theta} \, |\psi_{\beta\boldsymbol{\theta}\sigma}(\boldsymbol{r})|^2 f(E_{\beta\boldsymbol{\theta}\sigma} - \mu), \quad (6)$$

where the $\boldsymbol{\theta}$-integration is over the two-dimensional unit cell in reciprocal space, f is the Fermi equilibrium distribution with the chemical potential μ, and $E_{\beta\boldsymbol{\theta}\sigma}$ the energy spectrum of the QEDFT Hamiltonian H Eq. (3), where $\sigma = \uparrow$ or $\downarrow$ is the spin label. We choose the temperature $T = 1.0$ K. The Zeeman Hamiltonian is $H_{\text{Zee}} = \pm g^* \mu_{\text{B}}^* B/2$, and we use GaAs parameters $m^* = 0.067 m_e$, $\kappa = 12.4$, and $g^* = 0.44$.

The potential describing the exchange and correlation effects of the Coulomb interaction of the electrons,

$$V_{\text{xc},\sigma}(\boldsymbol{r}, B) = \frac{\partial}{\partial n_\sigma}(n_e \epsilon_{\text{xc}}[n_\uparrow, n_\downarrow, B])|_{n_\sigma = n_\sigma(r)}, \quad (7)$$

is derived from the Coulomb exchange and correlation functionals listed in Appendix A. The exchange and correlation contribution to the Coulomb interaction and the positive background charge make the localization of several electrons possible in a quantum dot.

In Appendix B, we detail how we adopt the exchange and correlation functional for a 2DEG in a perpendicular magnetic field and slightly modify the gradient-based exchange and correlation functional presented recently by Flick [22] for the interaction of electrons with the photon field in a cavity. We assume the reflective plates of the cavity to be parallel to the 2DEG and use the dipole approximation assuming the wavelength of the FIR field to be much larger than the lattice length L. We furthermore assume the cavity plates to be disks in order not to promote a preferred polarization of the electric component of the cavity photon field. We emphasize that even though we do select one photon mode here, nothing is specified about the number of photons present in the cavity in different situations. The functional can be expressed as

$$E_{\text{xc}}^{\text{GA}}[n, \nabla n] = \frac{1}{16\pi} \sum_{\alpha=1}^{N_p} |\lambda_\alpha|^2$$
$$\times \int d\boldsymbol{r} \frac{\hbar\omega_p(\boldsymbol{r})}{\sqrt{(\hbar\omega_p(\boldsymbol{r}))^2/3 + (\hbar\omega_g(\boldsymbol{r}))^2} + \hbar\omega_\alpha}, \quad (8)$$

where $\hbar\omega_\alpha$ and λ_α are the energy and coupling strength of cavity-photon mode α, respectively. N_p is the number of cavity modes. The coupling strength is expressed here in units of meV$^{1/2}$/nm as is explained in Appendix B. The gap-energy [21,22,24] stemming from considerations of dynamic dipole

polarizability leading to the van der Waals interaction is given by

$$(\hbar\omega_g(\boldsymbol{r}))^2 = C\left|\frac{\boldsymbol{\nabla} n_e}{n_e}\right|^4 \frac{\hbar^2}{m^{*2}} = C(\hbar\omega_c)^2 l^4 \left|\frac{\boldsymbol{\nabla} n_e}{n_e}\right|^4, \quad (9)$$

with $C = 0.0089$ and the cyclotron frequency $\omega_c = eB/(m^*c)$. We remind the reader here that even though the electron gas is considered 2D, the electrodynamics remain 3D. The dispersion of a magnetoplasmon confined to two dimensions is [33,34]

$$(\hbar\omega_p(q))^2 = (\hbar\omega_c)^2 + \frac{2\pi n_e^2}{m^*\kappa}q + \frac{3}{4}v_F^2 q^2, \quad (10)$$

where v_F is the Fermi velocity, and q is a general wave vector. Importantly, the plasmon at low magnetic field is almost gapless, indicating that the 2DEG is softer, regarding external perturbation, than a 3D electron gas. To construct a local plasmon dispersion, we use the commonly used relation in this context that $q \approx k_F/6 \approx |\boldsymbol{\nabla} n_e|/n_e$ [35,36] and obtain

$$(\hbar\omega_p(\boldsymbol{r}))^2 = (\hbar\omega_c)(2\pi l^2 n_e(\boldsymbol{r}))\left(\frac{e^2}{\kappa l}\right)\left(l\frac{|\boldsymbol{\nabla} n_e|}{n_e}\right)$$
$$+ (\hbar\omega_c)^2\left\{\frac{1}{36}\left(\frac{|l\boldsymbol{\nabla} n_e|}{n_e}\right)^4 + 1\right\}, \quad (11)$$

where the dimensional information is made explicit by collecting terms into bracket pairs. Here, it becomes clear that for the 2D case we need all the terms specified for the magnetoplasmon to keep the treatment of the gap energy and the magnetoplasmon on equal footing. The exchange and correlation potentials for the electron-photon interaction are generated using the variation

$$V_{xc}^{EM} = \frac{\delta E_{xc}^{GA}}{\delta n_e} = \left\{\frac{\partial}{\partial n_e} - \boldsymbol{\nabla}\cdot\frac{\partial}{\partial \boldsymbol{\nabla} n_e}\right\}E_{xc}^{GA}, \quad (12)$$

together with the general extension to spin densities [35]:

$$E_{xc}[n_\uparrow, n_\downarrow] = \frac{1}{2}E_{xc}[2n_\uparrow] + \frac{1}{2}E_{xc}[2n_\downarrow] \quad (13)$$

and

$$\frac{\delta E_{xc}[n_\uparrow, n_\downarrow]}{\delta n_\sigma} = \left.\frac{\delta E_{xc}[n_e]}{\delta n_e(\boldsymbol{r})}\right|_{n_e(\boldsymbol{r})=2n_\sigma(\boldsymbol{r})}. \quad (14)$$

The electron-photon exchange-correlation potentials (12) are added to the DFT self-consistency iterations.

As the equilibrium electron spin densities are periodic, all matrix elements can be related to analytical matrix elements of phase factors $\exp(-i\boldsymbol{G}\cdot\boldsymbol{r})$ in the original Ferrari basis [30,32]. Thus it is convenient to construct the various gradient terms of the electron spin densities using their Fourier transforms to minimize the computational errors.

In constructing the exchange and correlation functional Eq. (8), Flick combines contributions due to the para- and diamagnetic electron-photon interactions Eq. (B6) up to second order in the coupling strength, noting that "physically such an approximation corresponds to including one-photon exchange processes explicitly, while neglecting higher order processes," to use his words [22]. Importantly, the self-consistency requirement in our calculations thus bring into play higher order effects of repeated single photon processes.

The orbital and the spin components of the magnetization of the system are

$$M_o + M_s = \frac{1}{2c\mathcal{A}}\int_{\mathcal{A}} d\boldsymbol{r}\,(\boldsymbol{r}\times\mathbf{j}(\boldsymbol{r}))\cdot\hat{\mathbf{e}}_z$$
$$- \frac{g^*\mu_B^*}{\mathcal{A}}\int_{\mathcal{A}} d\boldsymbol{r}\,\sigma_z(\mathbf{r}), \quad (15)$$

where $\mathcal{A} = L^2$ is the area of a unit cell in the system, and the current density is given by Eq. (B2) in Appendix B. The magnetization is an equilibrium quantity well suited to investigate the effects of the coupling of the FIR photon modes of the cavity to the 2DEG.

III. RESULTS

For all calculations, unless use of other values is indicated, we use ten Landau bands (each split into pq subbands) and a 16×16 (θ_1, θ_2)-mesh for a repeated four-point Gaussian quadrature in the primitive zone of the reciprocal lattice. For the spatial coordinates, we use a 40×40 (x, y) mesh for a repeated four-point Gaussian quadrature. For all the calculations, we consider only one FIR photon cavity mode with energy $\hbar\omega_\alpha = 1.0$ meV. For clarity, we keep the notation for the energy of the mode as $\hbar\omega_\alpha$ and the coupling as λ_α, even though the index α could have been dropped.

In the upper panel of Fig. 1, the periodic dot potential is displayed for four unit cells of the square lattice. In the lower panel of the figure is the corresponding electron density for two electrons, $N_e = 2$, in each unit cell or dot for one quantum of magnetic flux, $pq = 1$, through a unit cell corresponding to the magnetic field $B = 0.414$ T. The electron-photon coupling strength is $\lambda_\alpha l = 0.050$ meV$^{1/2}$. Clearly, even at this low magnetic field, the overlap of the electron density between the dots is very low, i.e., the electrons are well localized in the dots. This is facilitated by the homogeneous positive background charge density in the plane of the 2DEG and the effects of the exchange and correlation functional for the electron-electron Coulomb interaction.

For a higher magnetic field, the two electrons are even better confined within the dot potential as the magnetic length l is then smaller compared to the lattice length L. In the upper panel of Fig. 2, the exchange and correlation potential $V_{ex,\downarrow}(\boldsymbol{r})$ Eq. (A5) is shown for $pq = 4$ and $\lambda_\alpha l = 0.050$ meV$^{1/2}$. Note the depth of the potential compared to the maximum depth of the confinement potential, $V_0 = -16$ meV. In the lower panel of Fig. 2 is the exchange and correlation potential $V_{xc,\downarrow}^{EM}(\boldsymbol{r})$ Eq. (12). The interaction with the photon field with an isotropic distribution of a polarization vector tends to spread the electron charge density as has been seen in calculations, where exact diagonalization (or configuration interaction) methods have been used to describe the electron cavity-photon interactions [37,38]. This action of $V_{xc,\downarrow}^{EM}(\boldsymbol{r})$ to polarize or spread the charge explains the attractive part seen in the lower panel of Fig. 2 forming a ring structure where the ratio of the gradients of the electron density versus the density itself are high. This behavior is expected as such terms are numerous in the potentials. The relative sharpness of the structures in $V_{xc,\downarrow}^{EM}(\boldsymbol{r})$ makes a strong requirement of including a high number of Fourier coefficients in the numerical
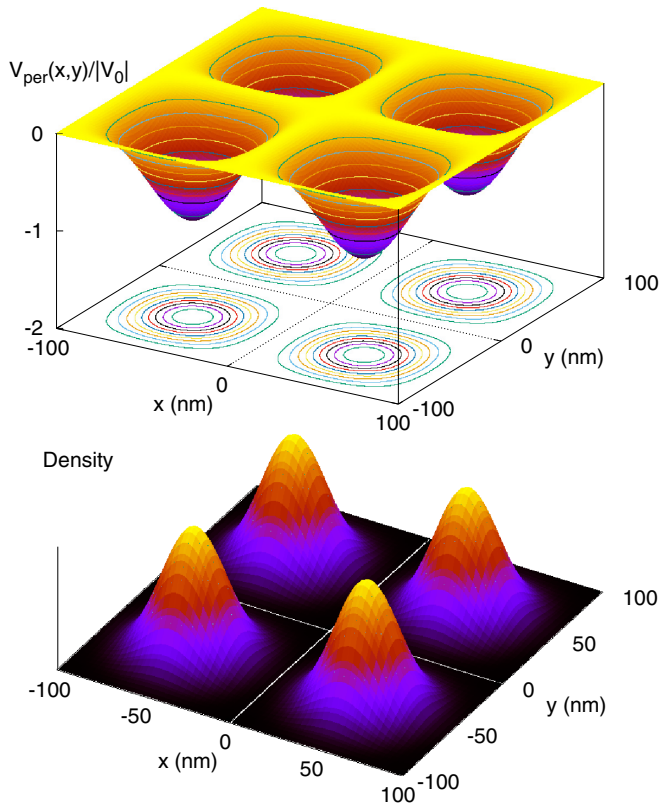
FIG. 1. For four unit cells of the square lattice, the dot confinement potential (upper panel) and the electron density for two electrons (lower panel), $N_e = 2$, in each dot for $pq = 1$ corresponding to $B = 0.414$ T. $\lambda_\alpha l = 0.050$ meV$^{1/2}$, $\hbar\omega_\alpha = 1.0$ meV, $L = 100$ nm, $\kappa = 12.4$, $T = 1.0$ K, $V_0 = -16.0$ meV, $g^* = 0.44$, and $m^* = 0.067 m_e$.

FIG. 2. The exchange and correlation potentials for the mutual electron Coulomb interaction V_{xc} (upper panel) and the electron-photon interaction $V_{\text{xc}}^{\text{EM}}$ (lower panel) for $N_e = 2$, $pq = 4$, $\lambda_\alpha l = 0.050$ meV$^{1/2}$ and $\hbar\omega_\alpha = 1.0$ meV. The potentials are shown for the lower energy spin direction.

calculations, much higher than is needed for $V_{\text{ex},\downarrow}(\mathbf{r})$. When the number of electrons in the unit cell, N_e, is increased, the potentials start to acquire square-symmetry aspects from the lattice with their characteristics deviating from the circular symmetry that has the upper hand in Fig. 2.

In Fig. 3, the polarization of the charge distribution defined as $[n_e(\lambda) - n_e(0)]l^2$ is displayed for both $N_e = 2$ (upper panel) and $N_e = 4$ (lower panel), with $\lambda_\alpha l = 0$ to 0.050 meV$^{1/2}$ and $pq = 4$. Clearly, for $N_e = 2$, the polarization of the charge is isotropic like the distribution of the polarization vector of the photon field. Moreover, we see clearly how charge is moved away from the center of the dot to its outskirts. The lower panel of Fig. 3 shows that for the higher number of electrons $N_e = 4$ in the dots, the charge polarized by the cavity photon field is not anymore isotropic, but has assumed to a large extent the square symmetry of the underlying square dot lattice. This is understandable as it is energetically favorable to relocate some of the charge to the corner regions of the unit cell due to the strong direct Coulomb repulsion, but still charge is polarized away from the center region of the dots.

We are investigating a periodic 2DEG here, so especially at high magnetic fields, we expect the energy bands formed by the lattice periodicity to be narrow for the states of electrons that are well localized in the dots, and higher up in the
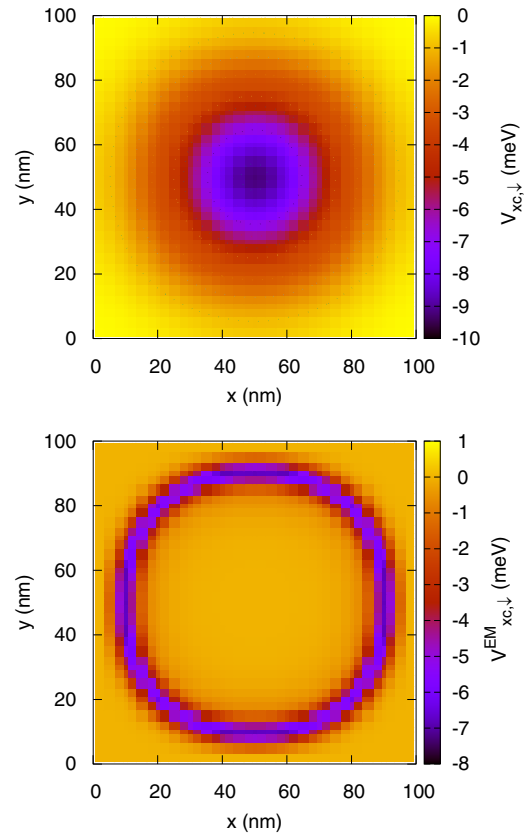
energy spectra they can be expected to broaden. Exactly, this behavior can help us to get insight into what is happening in the system as the electron photon coupling is changed. To prepare for this analysis, we show the eight lowest energy bands for $N_e = 2$ at $pq = 1$ and $\lambda_\alpha l = 0.050$ meV$^{1/2}$ in Fig. 4. Notice that for $pq = 1$ $B = 0.414$ T and for $g^* = 0.44$, the spin splitting of the bands is not clearly resolved in Fig. 4, but we see a large energy gap from the two lowest occupied bands showing holelike dispersion to the higher unoccupied bands with electronlike dispersion. The two lowest bands have only a small dispersion, indicating the localization of the electrons in the quantum dots, but the higher ones have a large one. The chemical potential $\mu = -8.954$ meV located in the gap between the occupied and the unoccupied bands. We remind the reader that even when using terms like holelike character, we are only modeling electrons in the conduction band of a GaAs heterstructure.

In this self-consistent QEDFT model of a 2DEG interacting with the modes of a photon cavity, the chemical potential μ shifts nontrivially with the interaction strength. This is not unexpected for DFT calculation, but in Fig. 5 we plot $(E_{\beta\theta\sigma} - \mu)$ for the eight lowest energy bands (shown in Fig. 4) as a function of the electron-photon coupling strength $\lambda_\alpha l$. We remember that for $pq = 1$ the band dispersion is much larger than the Zeeman spin splitting, so in each panel of Fig. 5 there
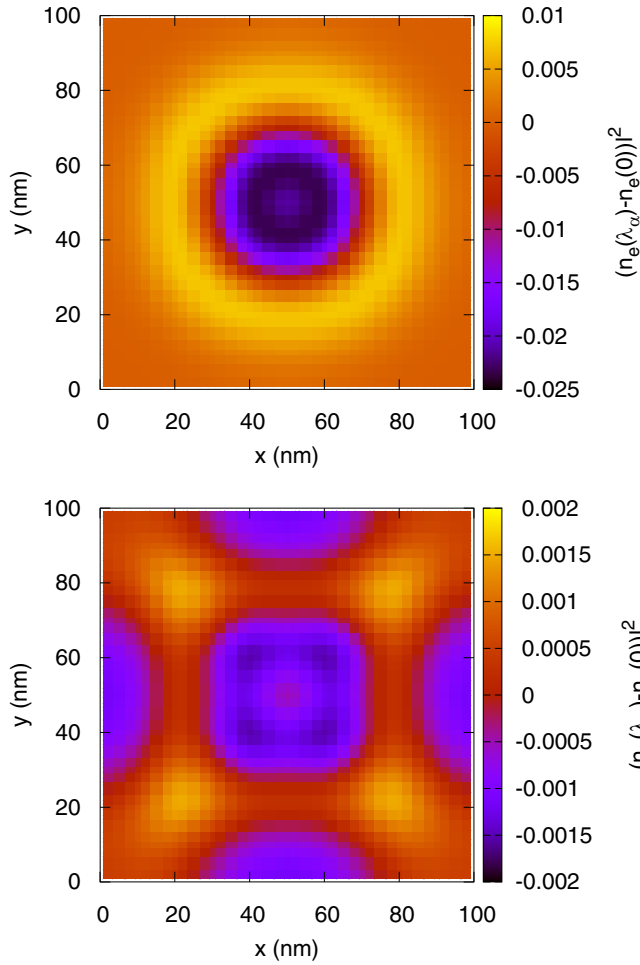
FIG. 3. The change in the electron density $[n_e(\lambda_\alpha) - n_e(0)]l^2$ for the electron-photon coupling $\lambda_\alpha l = 0.050$ meV$^{1/2}$ compared to the density without the coupling ($\lambda_\alpha l = 0$) for $N_e = 2$ (upper panel), and $N_e = 4$ (lower panel). $pq = 4$, and $\hbar\omega_\alpha = 1.0$ meV.

FIG. 4. The four lowest in energy bands for $pq = 1$ and $\lambda_\alpha l = 0.050$ meV$^{1/2}$. Each band is composed of two spin subbands separated by the Zeeman energy 1.053×10^{-2} meV. As $N_e = 2$, the chemical potential $\mu = -8.954$ meV is located in the gap between the filled bands showing holelike character below, and the empty bands showing electronlike character above. $T = 1.0$ K. $\hbar\omega_\alpha = 1.0$ meV.

are two bands. The lower left panel shows the two bands with highest occupation, and the other panels show higher lying bands that are almost unoccupied, as here, $T = 1.0$ K, giving the thermal energy $k_B T \approx 0.086$ meV.

In a many-body calculation of interacting electrons and photons, one utilizes a Fock-basis of states that include both states from the original electron and photon bases [37,38]. The resulting states are referred to as photon dressed states, and commonly the term photon replicas is used. Here, the DFT orbitals or states are derived in a different way, but it may still be appropriate to talk about photon-dressed electrons, that are fermions, but no photon replicas are identifiable. But a look at the left panels of Fig. 5 should remind us of another phenomena, a *FIR magnetoplasmon polariton*. The reduction of the gap between the energy bands seen in the left panels of Fig. 5 is reminiscent of the formation of a bosonic magnetoplasmon polariton composed of a cavity photon mode and the polarization of charge across a gap in the energy spectrum. We emphasize that our DFT results cannot be taken as a proof of the emergence of a magnetoplasmon polariton, but we take them as an indication. Additionally, we point out that concurrently to the narrowing of the band gap or gaps, the
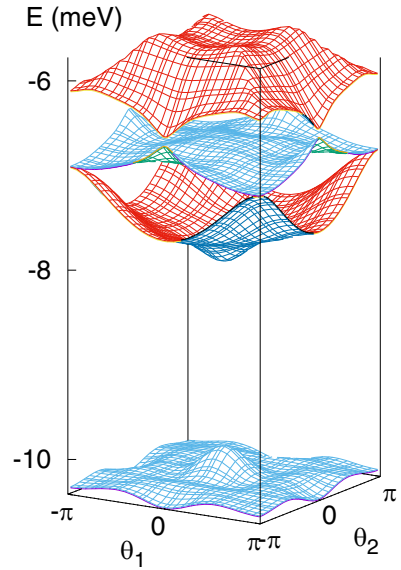
mixing of the states of the original basis functions increases beyond what is caused by the Coulomb interaction alone. The electron-photon interaction is leading to a mixing of energy bands as seen in the formation of a magnetoplasmon polariton. A corresponding structure is found in the energy spectrum of the 2DEG for higher values of the magnetic flux pq.

The electron-photon coupling is expected to increase the total energy for the electronic system, but in a dot-modulated charge neutral 2DEG this can be hidden by other details. In Fig. 6, we display in the top panel the total energy as a function of the number of electrons in a unit cell N_e, but also for the electron-photon coupling in the range $\lambda_\alpha l = 0 - 0.1$ meV$^{1/2}$. Clearly, it is difficult to discern the effects of the coupling here. They become clearer in the center panel for $pq = 1$ and the bottom panel for $pq = 4$, where we display $E_{\text{total}}(\lambda) - E_{\text{total}}(0)$ as a function of $\lambda_\alpha l$ for several values of N_e. As expected, the electron-photon coupling leads to an increase in the total energy of the system. The largest effects for the increase of the total energy is for $N_e = 1$ or 2 for $pq = 1$ (center panel). The increase for $N_e = 3$ or 4 is much smaller, which can be referred back to the decreased polarizability of the electron charge for the higher number of electrons. Here, the shell structure of the quantum dots, and the availability of un- or partially occupied states close to the chemical potential is important to facilitate the polarization. For $pq = 4$ (bottom panel) similar behavior is found, but there the increase in the total energy is still rather high for $N_e = 3$, which reflects the change in the shell structure with a higher magnetic field.

The magnetization for a dot-modulated 2DEG without the coupling to cavity modes is presented in Fig. 7. Note the difference in scales for the orbital component and the spin component due to the GaAs parameters used. In Fig. 7, we
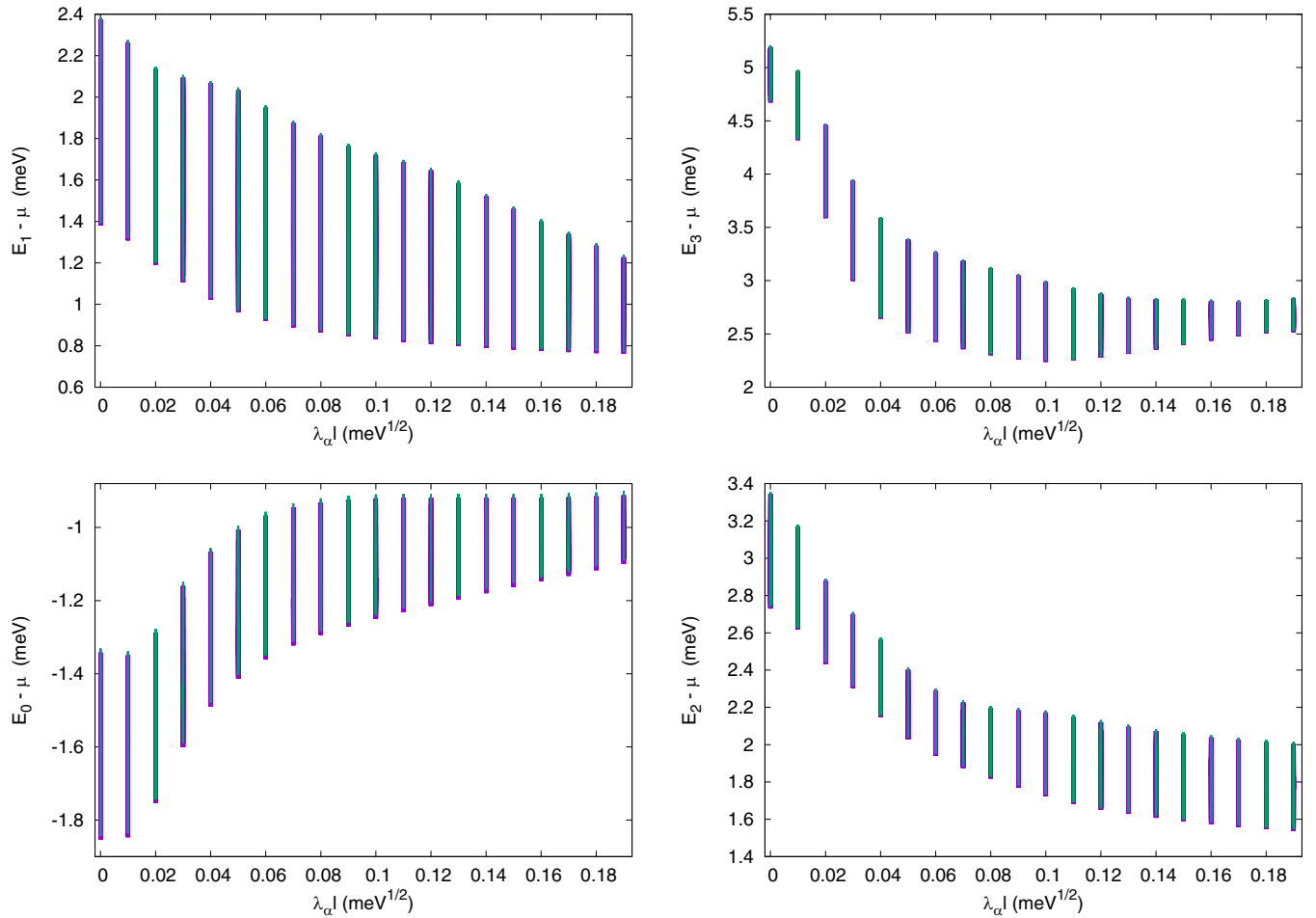
FIG. 5. The dispersion of the four lowest energy bands as a function of the electron-photon coupling. The two overlapping spin components for the lowest band (bottom left), the second band (top left), the third band (bottom right), and the fourth one (top right) are displayed with two different colors. $pq = 1$, and μ is the chemical potential at $T = 1.0$ K. $\hbar\omega_\alpha = 1.0$ meV.

show that in the absence of the electron-photon interaction, relatively few Fourier coefficients are need for the calculation. The notation $G_i^{\max} = 5$ indicates that the integers G_1 and G_2 specifying the reciprocal lattice vectors, $\boldsymbol{G} = G_1\boldsymbol{g}_1 + G_2\boldsymbol{g}_2$, are in the interval $-5, \ldots, 0, \ldots, 5$. For the calculations with $\lambda_\alpha l \neq 0$, we use $\max |G_i| = 12$ for $pq = 1$, and 15 for higher values of the flux pq.

The spin component of the magnetization, M_s, in Fig. 7 for $pq = 4$ vanishes for $N_e = 2, 4, 8$, corresponding to the filling factors $\nu = 1/2, 1$, and 2, respectively. For a system with no Coulomb interaction between the electrons, M_s also vanishes for $N_e = 6$, but here all parts of the Coulomb interaction, the direct one and the exchange and correlation contributions, cause a rearrangement of the spin structure around $N_e = 6$, corresponding to the filling factor $\nu = 3/2$. This happens in the same region as the orbital magnetization, M_o changes signs. M_o assumes local extrema values for the filling factors $\nu = 1$ and 2.

As the spin contribution to the magnetization is small for the GaAs parameters, we shall in what follows concentrate on the effects of the electron-photon coupling on the orbital magnetization. In Fig. 8, we display, for an overview, M_o as a function of N_e for values of the electron-photon coupling strength $\lambda_\alpha l$ in the range of 0–0.1 meV$^{1/2}$ for four different

values of the magnetic flux pq. The filling factor ν is indicated on the upper abscissa of the subfigures.

Clearly, M_o is in certain cases influenced by the coupling $\lambda_\alpha l$ to a considerable amount, as could be expected from the structure of the integrand for the orbital term in Eq. (15). To make these changes more visible we plot $\Delta M_o = M_o(\lambda_\alpha) - M_o(0)$ as functions of $\lambda_\alpha l$ for four different values of the magnetic flux pq and the several values of N_e in Fig. 9. Like for the total energy displayed in Fig. 6, we notice that the largest changes in the orbital magnetization occur for one, two, or three electrons in each quantum dot, but here the largest change is always found for $N_e = 2$ with increasing coupling $\lambda_\alpha l$. The sign of $\Delta M_o(\lambda_\alpha)$ can be understood with a comparison with the information in Fig. 8.

We note that the shape of the curves for $\Delta M_o(\lambda_\alpha)$ is nontrivial. It depends on the filling factor, the magnetic flux pq, and the structures of the energy bands. A noteworthy feature of the orbital magnetization for a QD array characterized by small values of N_e is the sensitivity to the increase of $\lambda_\alpha l$, even in the weakly interacting regime. Indeed, for all four values of pq, one notices visible changes in the magnetization when the electron-photon coupling slightly increases to $\lambda_\alpha l = 0.02$. One also notices that for $N_e = 1, .., 3$ the deviations from the values corresponding to the noninteracting regime $\lambda_\alpha l = 0$ are
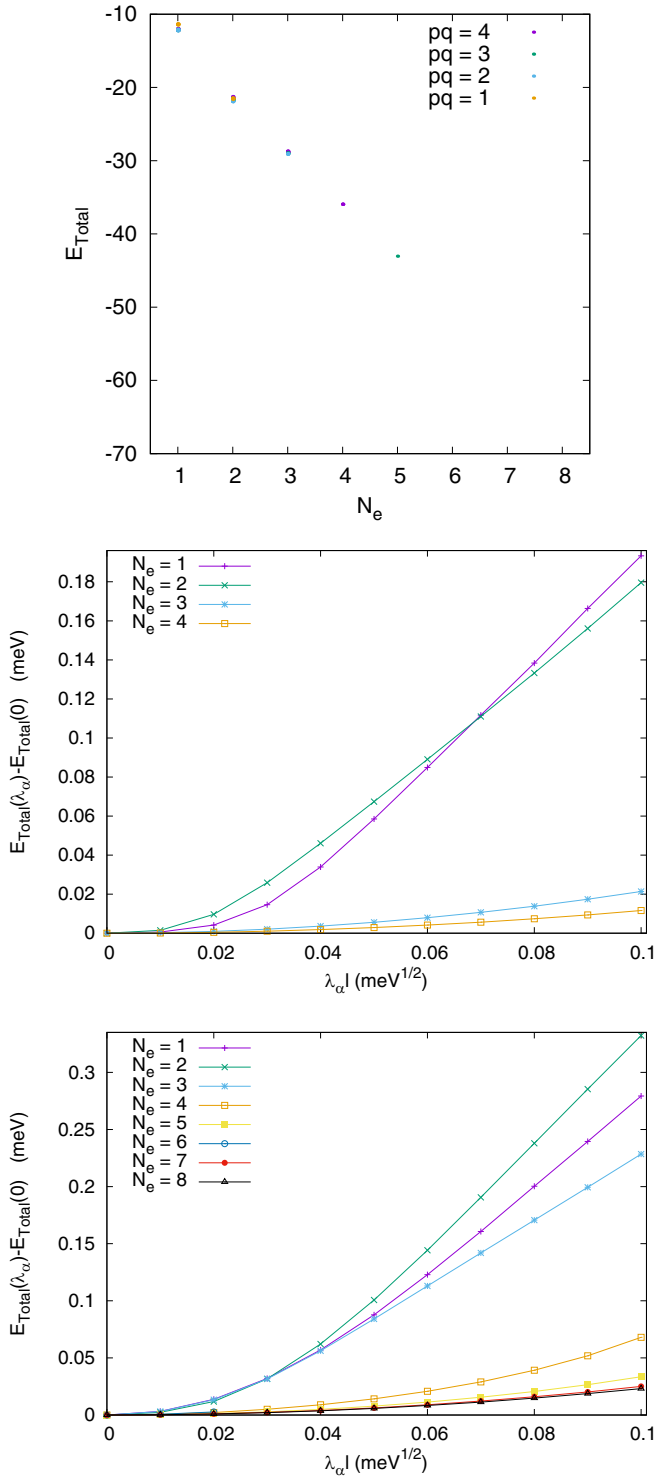
FIG. 7. The orbital M_o and the spin component of the magnetization M_s as functions of the number of electrons in a unit cell N_e. $\lambda_\alpha l = 0$, $T = 1.0$ K, $g^* = 0.44$, and $M_0 = \mu_B^*/L^2$.

response of the magnetization to the electron-photon coupling. For example, as pq increases, the magnetization of the three-electron QD array shows a stronger dependence on $\lambda_\alpha l$. This behavior suggests that in such a complex system the contribution of the coupling strength to equilibrium properties depends also on the configuration of the system, that is, charge distribution, energy bands, gaps, and magnetic field.

Even though only single-photon exchange processes were taken into account with terms up to second order in $\lambda_\alpha l$ in the construction of the exchange and correlation functional for the electron-photon interaction Eq. (13), the self-consistency required in the DFT calculation forms higher order processes built from the the single-photon exchange processes. On top of this, the underlying square dot lattice and the Coulomb interaction between the electrons have a strong influence.

IV. CONCLUSIONS

A self-consistent quantum-electrodynamical density-functional approach was developed and implemented for a square periodic quantum dot lattice placed in between the parallel plates of a far-infrared photon microcavity and subjected to an external perpendicular homogeneous magnetic field. The Coulomb interaction and the electron-photon coupling are treated self-consistently, while the exchange-correlation functionals are adapted for the GaAs 2DEG hosting the array. We explore how the interplay between the Coulomb interaction and the electron-photon coupling affects some equilibrium properties of the system.

In the presence of the cavity, the charge density of the system is polarized and its total energy increases with increasing electron-photon coupling. The orbital magnetization of the electron system changes in nontrivial ways, depending on the magnetic flux, the number of electrons in each dot, and their band structure. The dispersion of the energy bands closest to the chemical potential separating empty and filled states shows an indication for the emerging structure of magnetoplasmon-polaritons in the dots. The magnetization of the system is especially adequate to explore in future experiments as it is an equilibrium measurable quantity, only

FIG. 6. The total energy E_{total} as function of the number of electrons in each unit cell N_e for four different values of magnetic flux quanta pq and the electron-photon coupling strength $\lambda_\alpha l$ in the range from 0–0.1 meV$^{1/2}$ (top panel). The difference in the total energy $E_{\text{total}}(\lambda_\alpha) - E_{\text{total}}(0)$ as a function of $\lambda_\alpha l$ for $pq = 1$ (center panel), and $pq = 4$ (bottom panel). The spectrum in the top panel contains points for all values of the coupling strength $\lambda_\alpha l$ used for the construction of the lower panels. $T = 1.0$ K, and $\hbar\omega_\alpha = 1.0$ meV.

considerably enhanced as pq increases. On the other hand, the number of magnetic flux quanta pq also influences the
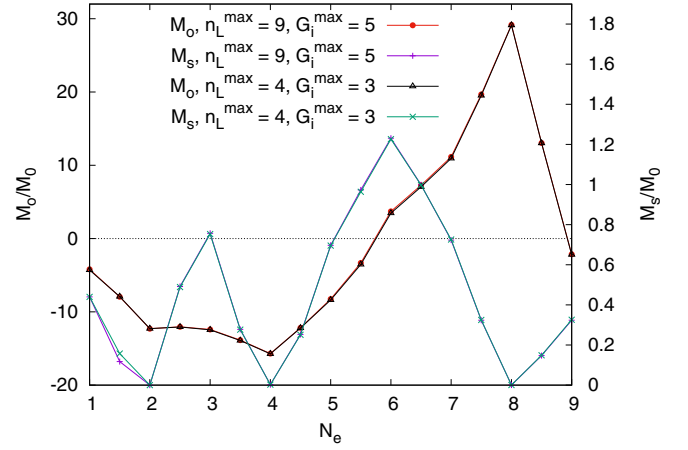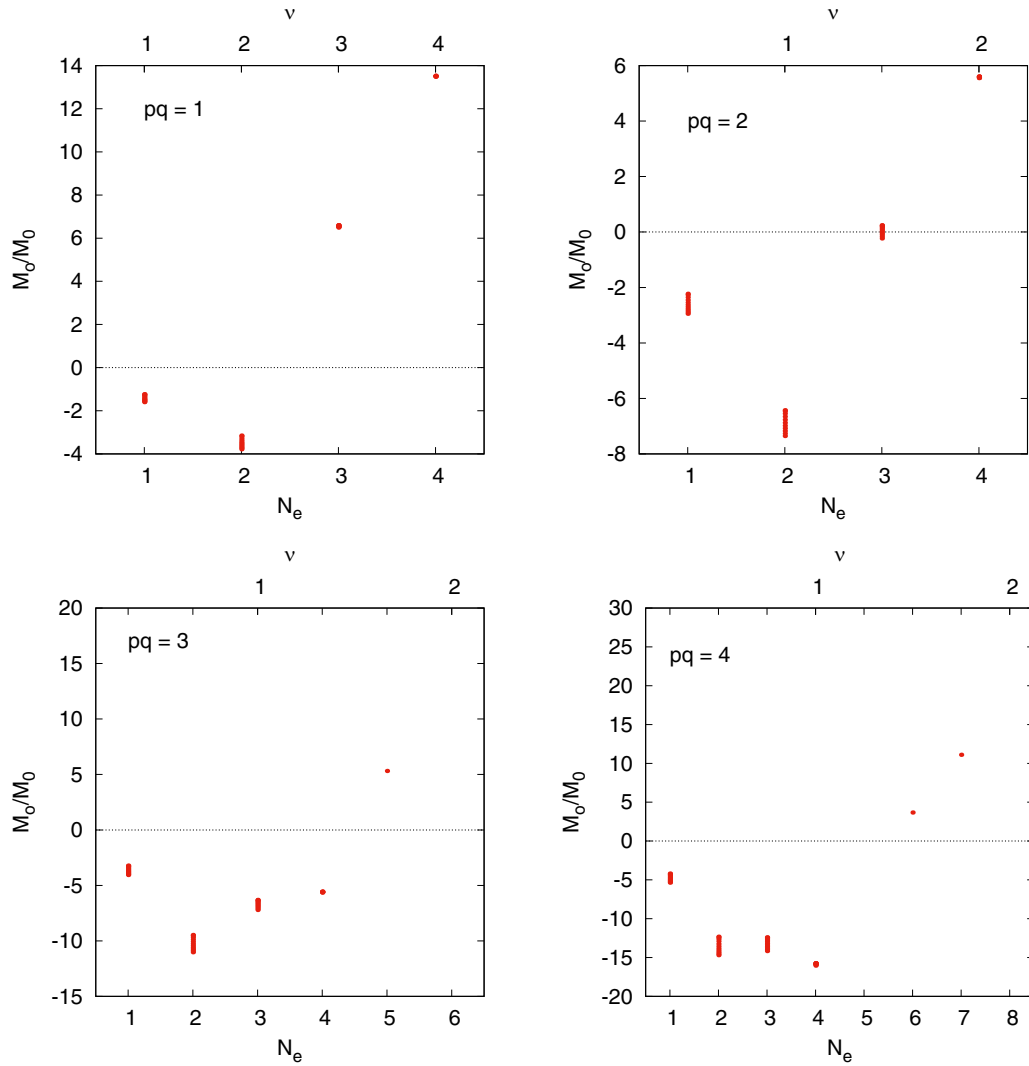
FIG. 8. The orbital magnetization M_o as a function of the number of electrons in a unit cell N_e for $pq = 1$ (upper left), $pq = 2$ (upper right), $pq = 3$ (bottom left), and $pq = 4$ (bottom right) for the electron-photon coupling strength $\lambda_\alpha l$ in the range from 0–0.1 meV$^{1/2}$. The filling factor ν is indicated by the top horizontal axes. $T = 1.0$ K, $\hbar\omega_\alpha = 1.0$ meV, and $M_0 = \mu_B^*/L^2$.

depending on its static properties. The orbital magnetization could thus be a good quantity to test the quality of the exchange and correlation functionals for the electron-photon interaction.

For a low number of electrons in each dot, the effects of the cavity photons can be seen in the polarizability of their charge distribution around their edges—this immediately brings forward the question about the interplay of the polarizability with the very well known compressible and incompressible stripes in the quantum Hall effect (QHE) regime [39–41]. We are not in the QHE regime as is best seen by comparison to the model calculation for the edge states in a QHE system within the Thomas-Fermi approximation (TFA) done by Lier and Gerhardts [42]. The characteristic length of our wave functions is the magnetic length l, that for $pq = 4$ is approximately 20 nm, much larger than the TFA screening length $a_B^*/2 \approx 5$ nm, half an effective Bohr radius, for GaAs. We would thus

need a much higher magnetic field, electron density, or lattice length for our array to enter the QHE regime. We are not sure our model could handle calculations well in this strict semiclassical QHE regime, which is well described within the TFA, without resorting to wave functions.

The exchange and correlation functional describing the effects of the cavity photons is constructed from the polarizability of the electron system and is thus related to its density response function as can be seen from the presence of the magnetoplasmon dispersion in the functional. But, again, we remind the reader that the induced density for five Hartree-interacting electrons in a quantum dot with similar parameters presented in Fig. 5 in Ref. [43] shows no stripes. Furthermore, the pinning of the Landau bands to the chemical potential, or the Fermi level, that accompanies the emergence of compressible and incompressible stripes [39–41,44] is not seen in the present calculations.
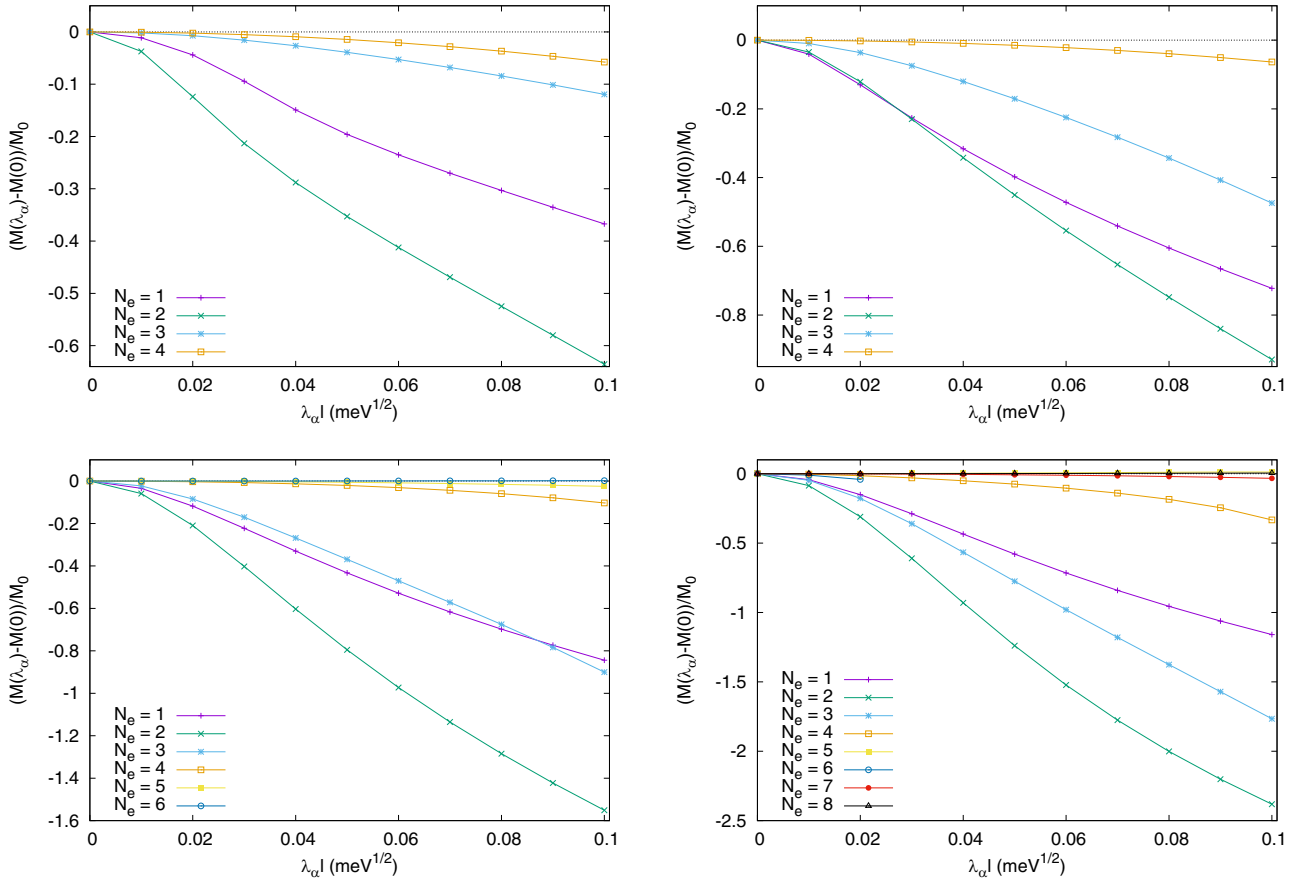
FIG. 9. The difference in the orbital magnetization $M_o(\lambda_\alpha) - M_o(0)$ as a function of the electron-photon coupling strength $\lambda_\alpha l$ for $pq = 1$ (upper left), $pq = 2$ (upper right), $pq = 3$ (bottom left), and $pq = 4$ (bottom right). $T = 1.0$ K, $\hbar\omega_\alpha = 1.0$ meV, and $M_0 = \mu_B^*/L^2$.

APPENDIX A: ELECTRON-ELECTRON COULOMB EXCHANGE AND CORRELATION FUNCTIONALS

The LSDA functional is a functional of the spin components of the electron density $n_e = n_\uparrow + n_\downarrow$, and the electron spin polarization expressed as $\zeta = (n_\uparrow - n_\downarrow)/n_e$. The functional has been interpolated between the nonpolarized and the ferromagnetic limit by Tanatar and Ceperley [45] for 2DEG. The form of the interpolation in 2D relies on work of Barth and Hedin [46] and Perdew and Zunger [47]:

$$f^i(\zeta) = \frac{(1+\zeta)^{3/2} + (1-\zeta)^{3/2} - 2}{2^{3/2} - 2}. \qquad (A1)$$

In an external magnetic field, it is more natural to replace the electron density with the local filling factor $\nu(\mathbf{r}) = 2\pi l^2 n_e(\mathbf{r})$ and the spin components thereof [48,49]. The exchange and correlation functional is then [50]

$$\epsilon_{xc}^B(\nu, \zeta) = \epsilon_{xc}^\infty(\nu)e^{-f(\nu)} + \epsilon_{xc}^0(\nu, \zeta)(1 - e^{-f(\nu)}), \qquad (A2)$$

where the interpolation between vanishing magnetic field and an infinite one depends on $f(\nu) = (3\nu/2) + 7\nu^4$ and the high field limit is $\epsilon_{xc}^\infty(\nu) = -0.782\sqrt{\nu}e^2/(\kappa l)$. The low magnetic field limit of the functional is

$$\epsilon_{xc}^0(\nu, \zeta) = \epsilon_{xc}(\nu, 0) + f^i(\zeta)[\epsilon_{xc}(\nu, 1) - \epsilon_{xc}(\nu, 0)]. \qquad (A3)$$

The exchange and correlation parts of the functional are separated, $\epsilon_{xc}(\nu, \zeta) = \epsilon_x(\nu, \zeta) + \epsilon_c(\nu, \zeta)$, with $\epsilon_x(\nu, 0) = -[4/(3\pi)]\sqrt{\nu}e^2/(\kappa l)$ and $\epsilon_x(\nu, 1) = -[4/(3\pi)]\sqrt{2\nu}e^2/(\kappa l)$. The parametrization of Ceperley and Tanatar for the correlation contribution part is expressed as [45]

$$\epsilon_c(\nu, \zeta) = a_0 \frac{1 + a_1 x}{1 + a_1 x + a_2 x^2 + a_3 x^3} Ry^*, \qquad (A4)$$

where $x = \sqrt{r_s} = (2/\nu)^{1/4}(l/a_B^*)^{1/2}$ and a_B^* is the effective Bohr radius. Optimized values for the correlation parameters a_i have been derived by Ceperley and Tanatar from a Monte Carlo calculation for the 2DEG [45]. In the new variables, ν and ζ, the exchange and correlation potentials are conve-

niently expressed as [48]

$$V_{\text{xc},\uparrow} = \frac{\partial}{\partial \nu}(\nu \epsilon_{\text{xc}}) + (1 - \zeta)\frac{\partial}{\partial \zeta}\epsilon_{\text{xc}},$$

$$V_{\text{xc},\downarrow} = \frac{\partial}{\partial \nu}(\nu \epsilon_{\text{xc}}) - (1 + \zeta)\frac{\partial}{\partial \zeta}\epsilon_{\text{xc}}. \quad (A5)$$

APPENDIX B: THE EXCHANGE AND CORRELATION FUNCTIONALS FOR THE ELECTRON-PHOTON INTERACTION

The electron-photon interaction with one photon mode labeled with α is described by

$$H_{\text{e-EM}} = -\frac{1}{c}\int d\mathbf{r}\,\mathbf{j}(\mathbf{r}) \cdot \mathbf{A}_\alpha(\mathbf{r})$$

$$+ \frac{e^2}{2m^*c^2}\int d\mathbf{r}\,n_e(\mathbf{r})A_\alpha^2(\mathbf{r}), \quad (B1)$$

with the current density

$$\mathbf{j}_{i\sigma}(\mathbf{r}) = -\frac{e}{m^*(2\pi)^2}\sum_\beta\int_{-\pi}^{\pi}d\theta\,\Re\{\psi_{\beta\theta\sigma}^*(\mathbf{r})\pi_i\psi_{\beta\theta\sigma}(\mathbf{r})\}$$

$$\times f(E_{\beta\theta\sigma} - \mu), \quad (B2)$$

where $i = x, y$ indicates its component along the cartesian spatial directions. We consider a parallel plates microcavity with the 2DEG plane in its center. As the wavelength of the FIR cavity photons is much larger than the lattice length L, we assume the the cavity vector potential in the dipole approximation to be described by

$$\mathbf{A}_\alpha = \mathbf{e}_\alpha\mathcal{A}_\alpha(a_\alpha^\dagger + a_\alpha), \quad (B3)$$

where $\mathbf{e}_\alpha$ is the polarization vector of the photon mode α with energy $\hbar\omega_a$. We will here assume the polarization uniform, as might be accomplished by a cylindrical cavity or in a rectangular cavity with equal horizontal lengths. Within these approximations, the electron-photon interaction can thus be expressed as

$$H_{\text{e-EM}} = \hbar\omega_c\Bigg[l\mathbf{I}\cdot\mathbf{e}_\alpha\bigg\{\bigg(\frac{e\mathcal{A}_\alpha}{c}\bigg)\frac{l}{\hbar}\bigg\}(a_\alpha^\dagger + a_\alpha)$$

$$+ N_e\bigg\{\bigg(\frac{e\mathcal{A}_\alpha}{c}\bigg)\frac{l}{\hbar}\bigg\}^2(a_\alpha^\dagger + a_\alpha)^2\Bigg], \quad (B4)$$

with the dimensionless spatial integral over the current density

$$l\mathbf{I}_i = \frac{1}{(2\pi)^2}\sum_{\beta\sigma}\int d\mathbf{r}\int_{-\pi}^{\pi}d\theta$$

$$\times \text{Re}\bigg\{\psi_{\beta\theta\sigma}^*(\mathbf{r})\bigg(\frac{l\pi_i}{\hbar}\bigg)\psi_{\beta\theta\sigma}(\mathbf{r})\bigg\}f(E_{\beta\theta\sigma} - \mu), \quad (B5)$$

where $i = x, y$. The ratio e/m^* characterizing the electromagnetic coupling is hidden in the cyclotron energy $\hbar\omega_c$, and the dimensionless quantity $(e\mathcal{A}_\alpha/c)(l/\hbar)$ appears in Eq. (B4) for both the para- and diamagnetic terms.

In the QEDFT literature, the electron-photon interaction within the dipole approximation is usually written as [22,51] for each photon mode,

$$H_{\text{int}} = -\omega_\alpha q_\alpha(\boldsymbol{\lambda}_\alpha \cdot \mathbf{R}) + \tfrac{1}{2}(\boldsymbol{\lambda}_\alpha \cdot \mathbf{R})^2, \quad (B6)$$

with

$$q_\alpha = \sqrt{\frac{\hbar}{2\omega_\alpha}}(a_\alpha^\dagger + a_\alpha). \quad (B7)$$

The coupling constant of the photon mode α for the electrons and the photons $\boldsymbol{\lambda}_\alpha$ includes the polarization of the vector potential and has the dimension of a square root of energy over length. A more common approach to the dipole approximation would have led us to replace $\mathbf{I}$ with the mean value of the spatial coordinate $\mathbf{R}$,

$$l^2\mathbf{I} \rightarrow \mathbf{R}, \quad (B8)$$

together with the identification

$$|\boldsymbol{\lambda}_\alpha| = \frac{\hbar\omega_c}{\sqrt{\hbar\omega_\alpha}}\frac{\sqrt{2}}{l}\bigg\{\bigg(\frac{e\mathcal{A}_\alpha}{c}\bigg)\frac{l}{\hbar}\bigg\} \quad (B9)$$

to make a connection to our presentation of the electron-photon interaction (B4). Here, we will thus determine the coupling $\lambda_\alpha l$ in units of $\sqrt{\text{meV}}$.

For the derivation of the exchange-correlation functional including single-photon exchange processes and terms up to $\sim\lambda_\alpha^2$, we point out the discussion of Flick [22], but after inspection of the dynamic electron polarizability $\alpha_{\mu\nu}(i\omega)$ introduced in Eq. (8) of Ref. [22], we select a dynamic polarizability for the isotropic 2DEG as

$$\alpha(iu) = \frac{\hbar}{4\pi}\int d\mathbf{r}\,\frac{\hbar\omega_p}{(\omega_p^2/3 + \omega_g^2 + u^2)\hbar^2} \quad (B10)$$

to obtain the needed dimensionality. The frequency integration for the exchange and correlation functionals expressed by Eqs. (7) and (9) in Ref. [22] then leads to the functional $E_{\text{xc}}^{\text{GA}}[n, \nabla n]$ displayed in Eq. (8).

One may question the use of the dipole approximation for the electron-photon interaction for an extended 2DEG in an external magnetic field. The feature lengths of the 2DEG system, the lattice length L of the quantum array, and the cyclotron radius l are much smaller than the wavelength of the photons in the FIR cavity, which is in the range of several tenths of micrometers. Second, one has to have in mind how the FIR-absorption of single dots or wires [52] or arrays of quantum dots [53–55] was successfully calculated earlier using the dipole interaction and compared to experiments. There, the external exciting field had no spatial variation radially but an angular pattern exciting dipole or higher order electrical modes—but the self-consistent local field correction acquired spatial variations due to the underlying system that resulted in, for example, the excitation of Bernstein and higher order modes.

---

[1] G. L. Paravicini-Bagliani, F. Appugliese, E. Richter, F. Valmorra, J. Keller, M. Beck, N. Bartolo, C. Rössler, T. Ihn, K. Ensslin, C. Ciuti, G. Scalari, and J. Faist, Nat. Phys. **15**, 186 (2019).

[2] T. Yoshie, A. Scherer, J. Hendrickson, G. Khitrova, H. M. Gibbs, G. Rupper, C. Ell, O. B. Shchekin, and D. G. Deppe, Nature (London) **432**, 200 (2004).

[3] Q. Zhang, M. Lou, X. Li, J. L. Reno, W. Pan, J. D. Watson, M. J. Manfra, and J. Kono, Nat. Phys. **12**, 1005 (2016).

[4] A. Stockklauser, P. Scarlino, J. V. Koski, S. Gasparinetti, C. K. Andersen, C. Reichl, W. Wegscheider, T. Ihn, K. Ensslin, and A. Wallraff, Phys. Rev. X **7**, 011030 (2017).

[5] V. Savona, Z. Hradil, A. Quattropani, and P. Schwendimann, Phys. Rev. B **49**, 8774 (1994).

[6] D. Dini, R. Köhler, A. Tredicucci, G. Biasiol, and L. Sorba, Phys. Rev. Lett. **90**, 116401 (2003).

[7] C. Ciuti, G. Bastard, and I. Carusotto, Phys. Rev. B **72**, 115303 (2005).

[8] O. Kyriienko, A. V. Kavokin, and I. A. Shelykh, Phys. Rev. Lett. **111**, 176401 (2013).

[9] J. A. Hutchison, T. Schwartz, C. Genet, E. Devaux, and T. W. Ebbesen, Angew. Chem., Int. Ed. **51**, 1592 (2012).

[10] F. J. Garcia-Vidal, C. Ciuti, and T. W. Ebbesen, Science **373**, eabd0336 (2021).

[11] A. Thomas, L. Lethuillier-Karl, K. Nagarajan, R. M. A. Vergauwe, J. George, T. Chervy, A. Shalabney, E. Devaux, C. Genet, J. Moran, and T. W. Ebbesen, Science **363**, 615 (2019).

[12] C. Schafer, J. Flick, E. Ronca, P. Narang, and Á. Rubio, arXiv:2104.12429

[13] E. T. Jaynes and F. W. Cummings, Proc. IEEE. **51**, 89 (1963).

[14] L. S. Bishop, J. M. Chow, J. Koch, A. A. Houck, M. H. Devoret, E. Thuneberg, S. M. Girvin, and R. J. Schoelkopf, Nat. Phys. **5**, 105 (2009).

[15] Emanuele G. Dalla Torre, S. Diehl, M. D. Lukin, S. Sachdev, and P. Strack, Phys. Rev. A **87**, 023831 (2013).

[16] V. Moldoveanu, A. Manolescu, and V. Gudmundsson, Entropy **21**, 731 (2019).

[17] M. Ruggenthaler, J. Flick, C. Pellegrini, H. Appel, I. V. Tokatly, and A. Rubio, Phys. Rev. A **90**, 012508 (2014).

[18] C. Schäfer, M. Ruggenthaler, and A. Rubio, Phys. Rev. A **98**, 043801 (2018).

[19] J. Flick, N. Rivera, and P. Narang, Nanophotonics **7**, 1479 (2018).

[20] J. Flick, D. M. Welakuh, M. Ruggenthaler, H. Appel, and A. Rubio, ACS Photonics **6**, 2757 (2019).

[21] O. A. Vydrov and T. Van Voorhis, Phys. Rev. A **81**, 062708 (2010).

[22] J. Flick, arXiv:2104.06980 [Phys. Rev. Lett. (to be published)].

[23] P. S. Venkataram, J. Hermann, A. Tkatchenko, and A. W. Rodriguez, Phys. Rev. Lett. **118**, 266802 (2017).

[24] O. A. Vydrov and T. Van Voorhis, Phys. Rev. Lett. **103**, 063004 (2009).

[25] I. Meinel, T. Hengstmann, D. Grundler, D. Heitmann, W. Wegscheider, and M. Bichler, Phys. Rev. Lett. **82**, 819 (1999).

[26] I. Meinel, D. Grundler, D. Heitmann, A. Manolescu, V. Gudmundsson, W. Wegscheider, and M. Bichler, Phys. Rev. B **64**, 121306(R) (2001).

[27] P. G. Harper, Proc. Phys. Soc., Sect. A **68**, 874 (1955).

[28] M. Y. Azbel', Zh. Eksp. Teor. Fiz. **46**, 929 (1964) [Sov. Phys. JETP **19**, 634 (1964)].

[29] R. D. Hofstadter, Phys. Rev. B **14**, 2239 (1976).

[30] R. Ferrari, Phys. Rev. B **42**, 4598 (1990).

[31] H. Silberbauer, J. Phys.: Condens. Matter **4**, 7355 (1992).

[32] V. Gudmundsson and R. R. Gerhardts, Phys. Rev. B **52**, 16744 (1995).

[33] F. Stern, Phys. Rev. Lett. **18**, 546 (1967).

[34] T. Ando, A. B. Fowler, and F. Stern, Rev. Mod. Phys. **54**, 437 (1982).

[35] J. P. Perdew and Y. Wang, Phys. Rev. B **33**, 8800 (1986).

[36] D. C. Langreth and M. J. Mehl, Phys. Rev. Lett. **47**, 446 (1981).

[37] V. Gudmundsson, A. Sitek, N. R. Abdullah, C.-S. Tang, and A. Manolescu, Ann. Phys. **528**, 394 (2016).

[38] J. Flick, H. Appel, M. Ruggenthaler, and A. Rubio, J. Chem. Theory Comput. **13**, 1616 (2017).

[39] D. B. Chklovskii, B. I. Shklovskii, and L. I. Glazman, Phys. Rev. B **46**, 4026 (1992).

[40] A. Efros, Solid State Commun. **67**, 1019 (1988).

[41] A. Efros, Solid State Commun. **70**, 253 (1989).

[42] K. Lier and R. R. Gerhardts, Phys. Rev. B **50**, 7757 (1994).

[43] R. Krahne, V. Gudmundsson, C. Heyn, and D. Heitmann, Phys. Rev. B **63**, 195303 (2001).

[44] U. Wulf, V. Gudmundsson, and R. R. Gerhardts, Phys. Rev. B **38**, 4218 (1988).

[45] B. Tanatar and D. M. Ceperley, Phys. Rev. B **39**, 5005 (1989).

[46] U. von Barth and L. Hedin, J. Phys. C **5**, 1629 (1972).

[47] J. P. Perdew and A. Zunger, Phys. Rev. B **23**, 5048 (1981).

[48] M. I. Lubin, O. Heinonen, and M. D. Johnson, Phys. Rev. B **56**, 10373 (1997).

[49] V. Gudmundsson, C.-S. Tang, and A. Manolescu, Phys. Rev. B **68**, 165343 (2003).

[50] M. Koskinen, M. Manninen, and S. M. Reimann, Phys. Rev. Lett. **79**, 1389 (1997).

[51] J. Flick, M. Ruggenthaler, H. Appel, and A. Rubio, Proc. Natl. Acad. Sci. USA **112**, 15285 (2015).

[52] V. Gudmundsson, A. Brataas, P. Grambow, B. Meurer, T. Kurth, and D. Heitmann, Phys. Rev. B **51**, 17744 (1995).

[53] V. Gudmundsson and R. R. Gerhardts, Phys. Rev. B **54**, R5223 (1996).

[54] C. Dahl, Phys. Rev. B **41**, 5763 (1990).

[55] C. Dahl, J. P. Kotthaus, H. Nickel, and W. Schlapp, Phys. Rev. B **48**, 15480 (1993).